A READY-TO-USE APPLICATION OF LASER-PLASMA ACCELERATORS USING GABOR LENSES

R.M. Nichols*, UROP student, Imperial College London

M. Aslaninejad, N.P. Dover[#], Z. Najmudin, J.K. Pozimski, Imperial College London

P. A. Posocco, Imperial College London / The Cockcroft Institute / Gunnar Nilssons Cancerstiftelse

Abstract

A realistic particle distribution for a proton beam generated by laser-plasma interaction is required in order to simulate its transport through a Gabor lens system intended for use in radiobiology experiments. A stack of radiochromic films were exposed to a laser-driven proton beam of 25 MeV at the Vulcan Petawatt Experiment at Rutherford Lab and subsequently analysed to find the energy deposited per film and therefore the energy spectrum of the beam. Combined with the information on the radial profile of the dose in the films, it was possible to generate an idealised particle distribution. This distribution was sampled and used as a realistic proton source in a simulation through the Gabor lens system published at IPAC'13, scaled down to 4 MeV to fit the radiobiology experiment requirements.

INTRODUCTION

An intense beam of ions is generated when a solid target, several microns thick, is irradiated by a high intensity laser pulse [eg. 1, 2]. In such a scheme, the laser ionises the surface of the target and accelerates electrons to high energies. These electrons travel through the target and upon exiting the target result in the generation of huge quasi-static electric fields, due to charge separation. This field accelerates the ions at the target surface, which are often protons, carbon and oxygen ions from the typical hydrocarbon layer on the target surface [3, 4].

Ion beams accelerated in this way have attracted interest in recent years due to their potential for use in radiotherapy and a number of other applications [5]. There has been considerable investment in recent years into hadron therapy, which can provide more targeted therapy for deep-seated tumours than conventional x-ray or electron radiotherapy. Current systems for proton therapy are extremely costly and laser-accelerated beams could offer in the long-term simple and compact treatment devices and therefore significantly reduce treatment costs. Meanwhile, while still requiring further development before being suitable for treatment, they are sufficient to allow biologists to study the effect particles produce in cells, and are already far more convenient than electrostatic accelerators commonly used for this purpose. Experimental radiobiology with particles is an area that has been only partially explored and with a strong impact on the modalities of particles delivery to patients and treatment outcomes.

We believe that laser-plasma accelerators of the current

generation combined with a novel optical system based on Gabor lenses [6] is an ideal candidate for this application. If proven effective, Gabor lenses can be scaled to higher energies and thus easily applied to future laser-driven particle sources in a clinical environment.

THE PARTICLE DISTRIBUTION

The Vulcan Petawatt laser was focused to a focal spot of 4 μm (FWHM) at 45 angle of incidence onto a 100 μm thick Al target. The resultant accelerated proton beam was diagnosed using a film stack positioned 7.4 cm from the target. The stack itself is 0.66 cm thick and consisted of Al shielding followed by layers of RadioChromic Films, which darken when exposed to dose, alternated with spacers of either Fe or Al.

The set of RCFs (data taken in 2012) were scanned and the intensity value for each pixel was converted to dose by calibrating with pixel intensity values of images of RCFs exposed to known doses of radiation.

Calibration of the Films

Calibration images were obtained by scanning RCFs that had been exposed in three separate experiments when films were exposed to known doses of radiation using the Scanditronix MC 40 cyclotron at the University of Birmingham. In the area selected, the median pixel value is found for each of the colour channels of the image. A median is used rather than a mean as it will not be affected by outliers (caused by, for example, dust on the film). These values are then compared to the dose known to have irradiated the calibration films.

The results of the calibration are shown in Figure 1, in which the pixel intensity values are plotted as function of their known doses. The red channel is more sensitive than the green or blue channels and so it reaches its saturation point at a much lower dose. Therefore the red channel was used for the lower doses and the blue channel for the higher doses. The calibration switch point between the two channels was chosen at 200 Gy.
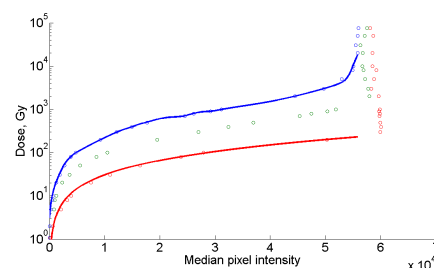
Figure 1: Calibration of how the red, green and blue channels of images of RCF respond to irradiation.

Image Conversion

For each processed image (an example in Figure 2), the image was disregarded if the mean intensity value over the entire film was less than twice the noise in the scanned image. Using this rule, only the first four RCF layers for this particular shot were used.
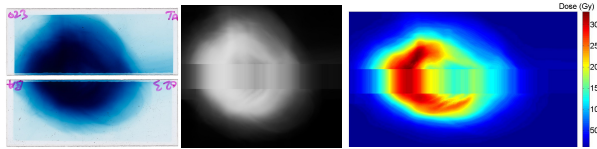
Figure 2: Scanned image of the first RCF (left), blue channel after processing (centre), dose map (right).

Reconstruction of the Energy Distribution

The dose deposited in each pixel of the scan of each RCF layer was calculated using the calibration. The mean dose in the layer was then converted to total energy deposited in the film's active layer, using the active layer density and thickness. For each of the four RCFs a profile of how much energy is deposited per proton in the active layer as a function of proton energy is generated using a series of TRIM Monte Carlo simulations [7].

The proton energy that dominates the energy deposition in each RCF is therefore found from the peak of the curves. To convert from energy deposited to the estimated proton number in the spectrum, the following initial assumptions were made:

- the area around the peak of the profile is selected using the 1/e width of the peak;
- inside this area protons of all energies deposit an equal amount of energy;
- protons with energies outside this area do not deposit any energy.

Therefore the energy deposited per proton is calculated by taking the average across this width. The number of protons in the beam depositing energy in each film is then given by the energy deposited in the film divided by the average energy deposited per proton in this peak. Hence the number of protons per MeV (dN/dE) is found by dividing the number of protons depositing energy by the width of the peaks in Figure 5. The number of protons at energies higher than 25 MeV, where the proton signal was below the noise, was set to zero.

Although the above assumptions give a good first estimate of the spectra, a large assumption is made by disregarding the dose deposited by the higher energy protons which could cause an overestimation of the particle numbers. Therefore, an iterative technique was used in which the initial spectral guess is convolved with the curve obtained with TRIM and the energy deposited in each film recalculated. The ratio of this new energy deposition value compared to the actual measured value is then found. The initial spectral guess is then modified by this ratio at each film layer, and this process is iterated until the energy deposited in each RCF calculated from the RCFs and the reconstructed energy spectrum was within 0.01%.
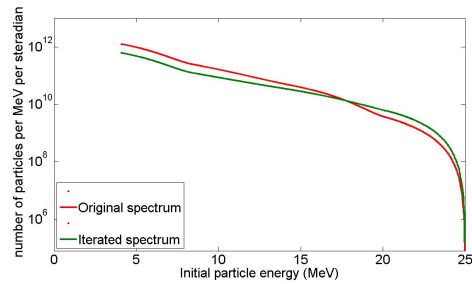
Figure 3: Comparison between the initial energy spectrum and the spectrum after iteration.

Reconstruction of the Transverse Distribution

The spreading of the beam in the direction transverse to the beam axis was assumed to be negligible over the depth of the stack (6.6 mm), as the distance between the films is less than 2% of the total distance travelled by the protons after the target. The mean transverse scattering within the stack was estimated from TRIM Monte Carlo simulations and was found to be $\sigma \approx 0.2$ mm for 35 MeV protons, negligible compared to the beam size.

The particle distribution was generated assuming that:

- the particles are emitted with cylindrical symmetry;
- the particles are emitted from a point like source;
- the particles are emitted at the same time, but with different energies;
- the particle distribution at each RCF is represented by a 2D Gaussian.

These assumptions reduce the 6D particle distribution to a 2D distribution (energy and radius). For each proton energy the particle number was first scaled with respect to the energy spectrum previously calculated. Then, a further modification depending on the spatial position was calculated by fitting a 2D Gaussian to the proton beam dose deposition profile (Figure 4). Below 5 MeV the distribution was given a spread similar to that of the first RCF in the stack.
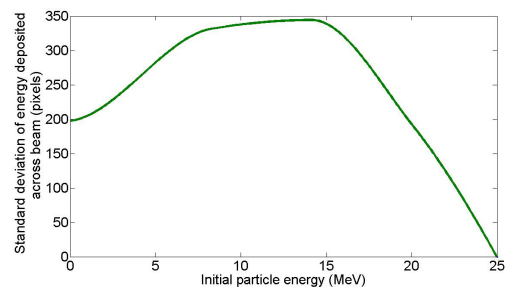
Figure 4: Spread of the dose distributed in the films as function of proton energy.

SIMULATION OF BEAM TRANSPORT

The particle distribution was converted into the GPT file format and used as input for the particle tracking simulations with GPT [8] using the lattice suggested in [6]. The preliminary results looked very unfavourable because the beam divergence is about 6 times larger than assumed and the number of particles above 10 MeV is too low for sufficient statistics (see Figure 5).

08 Medical Accelerators and Applications

A16 - Advanced Concepts

Therefore a new Gabor lens with the radius of anode and cathode increased from ~20 to 35 mm was designed and the lattice setup updated (Figure 6), increasing the acceptance angle by a factor of 3. Only 200 particles are initially available for the original distribution (see Figure 5-E red scale) in the lowest energy bin considered for experiments (4 MeV) at twice the divergence angle (~240 mrad half cone angle) compared with the angular acceptance (~120 mrad) of the improved lattice: the transmission is therefore below 25% (~50 particles at start). In order to boost the statistical significance of the results an artifical particle distribution (120 mrad divergence angle and 2100 particles per energy bin) was used for comparison.

The beam trajectory behind the aperture shown in Figure 6 is well defined after energy selection. For the artificial distribution ~80% of the particles in this energy bin are transmitted. The distribution derived from experiment show similar characteristics, but the overall transmission is 7.5%, equivalent to a 33% transmission through the aperture. Both distributions (see Figure 7) show a sharp peak at the chosen energy of 4 MeV with a FWHM below the bin width of 93.8 keV, which should be fine for most applications.
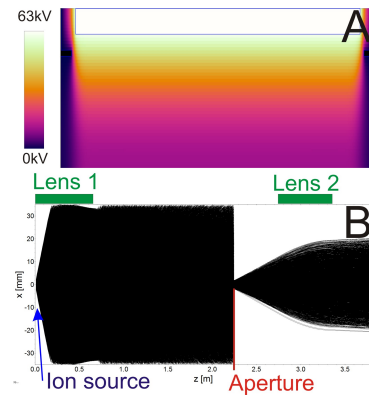
Figure 6: Lattice setup and a trajectory plot using a beam with ~120 mrad input divergence.
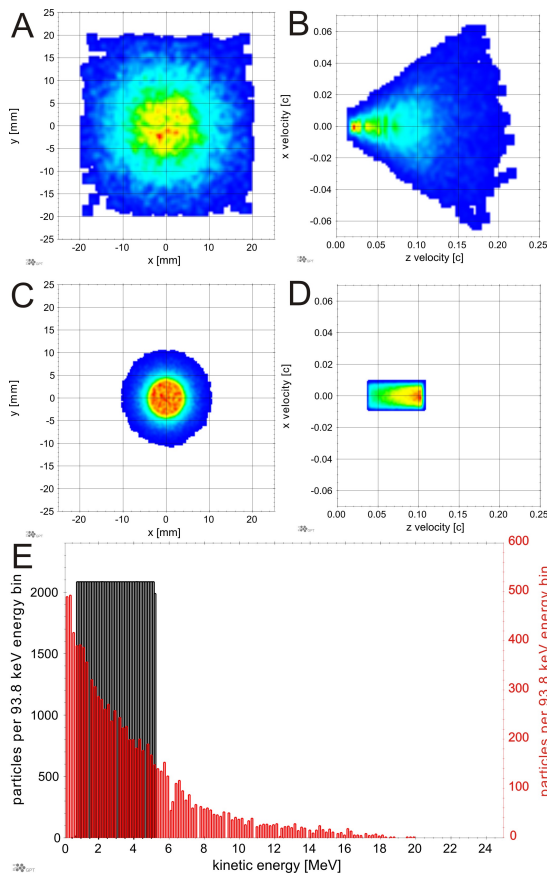
Figure 5: Graph A: transversal phase space (x,x') of the initial particle distribution and B the x-z velocity space both for the distribution generated experimentally; Graphs C and D: artificial distribution with reduced divergence angle and energy spread for comparison; Graph E: the particle number per energy bin for both distributions.
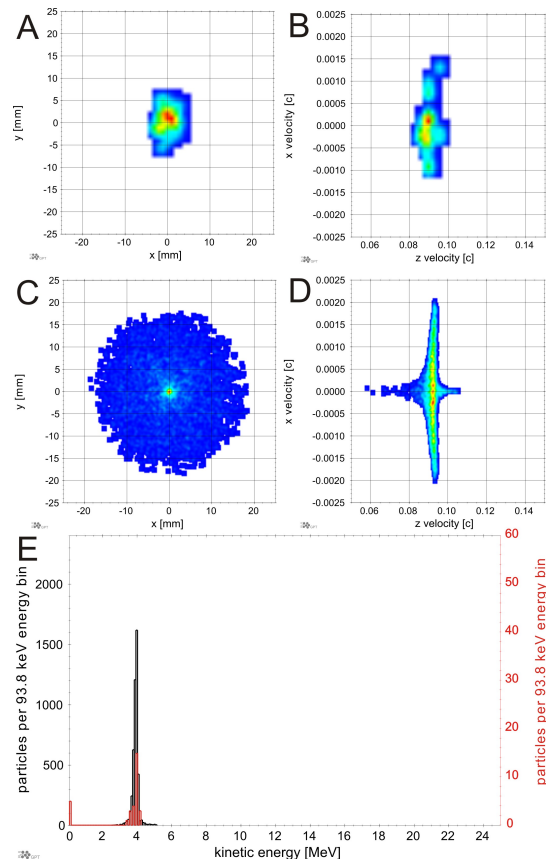
Figure 7: Graph A: transversal phase space (x,x') and B the x-z velocity space for the experimentally determined distribution after the aperture at 3.1 m; Graphs C and D: same plots for the artificial distribution.; Graph E: the particle number per energy bin for both distributions.

REFERENCES

[1] E. L. Clark, et al., Phys. Rev. Lett., 84, 2000.
[2] R. A. Snavely, et al., Phys. Rev. Lett., 85, 2000.
[3] A. Macchi, et al., Rev. Mod. Phys., 85, 2013.
[4] H. Daido, et al., Rep. Prog. Phys., 75, 2012.
[5] J. Fuchs, et al., Comptes Rendus Physique, 10, 2009.
[6] J. Pozimski and M. Aslaninejad. Laser and Particle Beams.
[7] J.F. Ziegler et al., "Stopping and range of ions in matter", 1985.
[8] 'General Particle Tracer', www.pulsar.nl/GPT/